JOURNAL OF GUIDANCE, CONTROL, AND DYNAMICS
Vol. 20, No. 5, September–October 1997

Optimal Low-Thrust Interception of Earth-Crossing Asteroids

Bruce A. Conway*
University of Illinois at Urbana–Champaign, Urbana, Illinois 61801

The spectacular collision of the Shoemaker–Levy 9 asteroid with Jupiter in July 1994 was a dramatic reminder of the inevitability of such catastrophes in the Earth's future unless steps are taken to develop methods for Earth-approaching object detection and possible interdiction. In this work, optimal (minimum-time) trajectories are determined for the interception of asteroids that pose a threat of collision with the Earth. An impulsive-thrust escape from the Earth is used initially to reduce flight time but is followed with continuous low-thrust propulsion using values of thrust and specific impulse representative of electric motors. The continuous optimization problem is formulated as a nonlinear programming problem using the collocation method in which the differential equations of motion are included as nonlinear constraint equations. The use of low-thrust propulsion after Earth escape is shown to dramatically decrease the mass of the interceptor vehicle at launch.

Introduction

THE spectacular collision of the Shoemaker–Levy 9 asteroid with Jupiter in July 1994 was a dramatic reminder of the fact that the Earth has experienced and will continue to experience such catastrophic events. Although the frequency of such massive collisions is very low, smaller objects collide with the Earth regularly and do damage that would be intolerable in any populated region. As an example, the Tunguska (Siberia) event of 1908 is estimated to have involved a 60-m object exploding at a height of 8 km and produced devastation over an area almost the same as that devastated by the eruption of Mount St. Helens.[1] The famous 1-km Meteor Crater in Arizona was made by the impact of an even smaller body only 30 m in diameter.[2] Human casualties due to direct meteorite strikes are rare but known.[3] The greater danger is due to the fact that the time between large impacts, such as the Tunguska impact, which released tens of megatons of TNT equivalent energy, is significant compared with a human lifetime, and there is a small chance that any impact will be in a populated area. The relative scarcity of such areas on the Earth may not offer the protection one might think as recent calculations suggest that larger bodies might do more damage if they did not hit land; predictions show that an impact anywhere in the Atlantic Ocean by a 400-m asteroid would devastate the (well-populated) coasts on both sides of the ocean with tsunamis over 60 m high.[4] A consensus is developing that although the probability for collision is low, the potential for destruction is immense, and thus some resources should be devoted to threat detection and possible interdiction.

The population of Earth-crossing objects is significant and continuously increasing by virtue of discovery. As of 1994, 163 Earth-crossing asteroids are known,[5] the largest being 1627 Ivar with a dimension of $\sim$8 km and mass of $\sim 10^{15}$ kg. (For comparison, the K/T or Cretaceous/Tertiary boundary impact of 65 million years ago, which left a $\sim$200 km crater, releasing an estimated 10^8 megatons equivalent energy in the Gulf of Mexico, would have been caused by a body $\sim$10 km in size.) The census of Earth-approaching asteroids is believed to be complete only for objects of Ivar's size; for bodies on the order of $\sim$1 km, the completeness of the census is estimated to be only $\sim$10%, based on the rate at which such objects continue to be discovered.[5] Twenty-six active Earth-crossing periodic comets are known, and they are similarly estimated to be 5–10% of the actual population. Two extinct Earth-crossing periodic comets are known, and because these are much more difficult to discover than active comets or large asteroids, it is estimated that there may be 10–20 extinct comets for each active comet. For the bodies whose orbits are accurately known, future close approaches can be determined. Table 1 is a partial list of comets and asteroids that will approach to within eight lunar distances in the next century.

Of course, it is the prevention of a catastrophic impact with which this paper is concerned. The dangerous object must be intercepted, at the earliest possible time, and then deflected or destroyed. This paper is not concerned with how the latter is accomplished; one strategy may be to detonate a large nuclear weapon near the surface of the asteroid or comet. In this work, optimal trajectories for the interception of dangerous asteroids are found. Low-thrust, high specific impulse propulsion is used because of the significant advantages it provides in propulsive mass required for a given mission. However, a low-thrust departure from Earth would require many revolutions of the Earth, which would consume a lot of time. It seems reasonable then to use an impulsive velocity change for the initial departure, followed by continuous low-thrust propulsion.

The analysis is necessarily three-dimensional as many of the Earth-crossing asteroids have significant inclinations. However, it simplifies the analysis to assume that, before the application of the departure impulse, the intercepting vehicle is in a low Earth circular orbit that lies in the ecliptic plane. The magnitude of this departure impulse is something that might in real life depend on the target and/or the capability of the launch vehicle. For this work, the departure impulse chosen is less than or equal in magnitude to that required for the most commonly employed interplanetary trajectory, i.e., the impulse required for escape from the Earth onto a Hohmann transfer ellipse to Mars, which yields a hyperbolic excess velocity ($v_{\infty/E}$) of 2.94 km/s. The optimizer may choose the point in the initial low Earth orbit from which to begin the departure. It may also choose the direction in which it is applied via in-plane and out-of-plane thrust pointing angles. The Earth is assumed to be in a circular orbit about the sun, and its true longitude on the departure date is found using the ephemeris program MICA from the U.S. Naval Observatory.[6] Specific impulse for the low-thrust motor is chosen from a range of values (2000–4000 s) representative of current technology.

Method

The variational equations used are those for the equinoctial elements. This avoids singularity of the elements for circular or equatorial orbits. The equinoctial elements and their relationship to the conventional elements are[7]

$$\begin{aligned} &a = a, \qquad P_1 = e\sin\tilde{\omega}, \qquad P_2 = e\cos\tilde{\omega} \\ &Q_1 = \tan(i/2)\sin\Omega, \qquad Q_2 = \tan(i/2)\cos\Omega \\ &\ell = \tilde{\omega} + M = \Omega + \omega + M \end{aligned} \tag{1}$$

The conventional elements are easily recovered using

$$\begin{aligned} &e = \sqrt{P_1^2 + P_2^2}, \qquad \Omega = \tan^{-1}(Q_1/Q_2) \\ &\tan(i/2) = \sqrt{Q_1^2 + Q_2^2} \end{aligned} \tag{2}$$

Received Sept. 10, 1996; revision received April 28, 1997; accepted for publication April 29, 1997.

*Professor, Department of Aeronautical and Astronautical Engineering. E-mail: bconway@uiuc.edu. Associate Fellow AIAA.

In these variables the variational equations become[7]

$$\frac{da}{dt} = \frac{2a^2}{h}\left[(P_2 \sin L - P_1 \cos L)R + \frac{p}{r}T\right]$$

$$\frac{dP_1}{dt} = \frac{r}{h}\left\{-\frac{p}{r}\cos L R + \left[P_1 + \left(1+\frac{p}{r}\right)\sin L\right]T - P_2(Q_1 \cos L - Q_2 \sin L)N\right\}$$

$$\frac{dP_2}{dt} = \frac{r}{h}\left\{\frac{p}{r}\sin L R + \left[P_2 + \left(1+\frac{p}{r}\right)\cos L\right]T - P_1(-Q_1 \cos L + Q_2 \sin L)N\right\} \tag{3}$$

$$\frac{dQ_1}{dt} = \frac{r}{2h}\left(1+Q_1^2+Q_2^2\right)\sin L\, N$$

$$\frac{dQ_2}{dt} = \frac{r}{2h}\left(1+Q_1^2+Q_2^2\right)\cos L\, N$$

$$\frac{d\ell}{dt} = n - \left[\frac{a}{a+b}\left(\frac{p}{h}\right)(P_1 \sin L + P_2 \cos L) + \frac{2b}{a}\right]R - \left[\frac{a}{a+b}\left(\frac{r}{h}+\frac{p}{h}\right)(P_1 \cos L - P_2 \sin L)\right]T - \left(\frac{r}{h}\right)(Q_1 \cos L - Q_2 \sin L)N$$

where

b = semiminor axis, $a\sqrt{(1-P_1^2-P_2^2)}$
F = acceleration produced by the low-thrust motor
h = angular momentum, nab
N = normal component of thrust acceleration, $F \sin\gamma$
n = mean motion, $\sqrt{(\mu/a^3)}$
R = radial component of thrust acceleration, $F \sin\beta \cos\gamma$
T = tangential component of thrust acceleration, $F \cos\beta \cos\gamma$

$$\frac{a}{a+b} = \frac{1}{1+\sqrt{1-P_1^2-P_2^2}}$$

$$\frac{p}{r} = 1 + P_1 \sin L + P_2 \cos L \tag{4}$$

$$\frac{r}{h} = \frac{h}{\mu(1+P_1 \sin L + P_2 \cos L)}$$

The control variables in the problem are the thrust pointing angles β and γ. Angle β is the in-plane thrust pointing angle; it is measured from the normal to the radius vector and is a positive angle if it yields a component of thrust pointing radially outward. Angle γ is the out-of-plane thrust pointing angle. It is positive if it yields a component of thrust in the direction of the orbital angular momentum.

The true longitude L is obtained from the mean longitude ℓ by first solving Kepler's equation in equinoctial variables,[7]

$$\ell = K + P_1 \cos K - P_2 \sin K \tag{5}$$

for the eccentric longitude K. Then the ratio r/a may be found as

$$r/a = 1 - P_1 \sin K - P_2 \cos K \tag{6}$$

The functions of eccentric longitude appearing in the variational equations are then determined as[7]

$$\sin L = (a/r)\left(\left\{1-[a/(a+b)]P_2^2\right\}\sin K + [a/(a+b)]P_1 P_2 \cos K - P_1\right)$$
$$\cos L = (a/r)\left(\left\{1-[a/(a+b)]P_1^2\right\}\cos K + [a/(a+b)]P_1 P_2 \sin K - P_2\right) \tag{7}$$

The thrust acceleration F varies as propellant is consumed; assuming a constant thrust motor,

$$\frac{dF}{dt} = \frac{F^2}{c} = \frac{F^2}{g I_{sp}} \tag{8}$$

where g is the acceleration of gravity at the Earth's surface, c is the motor exhaust velocity, and I_{sp} is the motor specific impulse (in seconds).

The problem is then to choose the time history of the thrust pointing angles β and γ to minimize the performance index, which is the time of flight, subject to satisfaction of the system variational equations (3), the system initial condition constraints

$$(a,\ P_1,\ P_2,\ Q_1,\ Q_2,\ \ell)$$

satisfying (at $t = 0$)

$$\bar{r} = \bar{r}_E, \qquad \bar{v} = \bar{v}_E + \bar{v}_{\infty/E} \tag{9}$$

(where $\bar{r}_E$ and $\bar{v}_E$ represent the position and velocity of the Earth, and $\bar{v}_{\infty/E}$ is the hyperbolic excess velocity of the spacecraft with respect to the Earth), and the terminal constraint (of interception)

$$(a,\ P_1,\ P_2,\ Q_1,\ Q_2,\ \ell)$$

satisfying (at $t = t_{final}$)

$$\bar{r} = \bar{r}_A \tag{10}$$

where the subscripts E and A refer to the Earth and the asteroid, respectively. The optimizer is free to choose two parameters that do not explicitly appear in the variational equations; two pointing angles, in-plane (β_0) and out-of-(ecliptic)-plane (γ_0) pointing angles that describe the direction of $\bar{v}_{\infty/E}$ following the impulsive Δv, which allows the vehicle to escape from low-Earth orbit.

The initial condition constraints (9) yield the following six scalar equations:

$$a_E \cos\theta_E - \frac{r\left[\cos L + \left(Q_2^2-Q_1^2\right)\cos L + 2Q_1Q_2 \sin L\right]}{1+Q_2^2+Q_1^2} = 0$$

$$a_E \sin\theta_E - \frac{r\left[\sin L - \left(Q_2^2-Q_1^2\right)\sin L + 2Q_1Q_2 \cos L\right]}{1+Q_2^2+Q_1^2} = 0, \qquad \frac{2r[Q_2 \sin L - Q_1 \cos L]}{1+Q_2^2+Q_1^2} = 0$$

$$\frac{\sqrt{\mu/p}\left[\sin L + \left(Q_2^2-Q_1^2\right)\sin L - 2Q_1Q_2\cos L + P_1 - 2P_2Q_1Q_2 + \left(Q_2^2-Q_1^2\right)P_1\right]}{1+Q_2^2+Q_1^2} - v_E \sin\theta_E + v_{\infty/E}\cos\gamma_0 \sin(\beta_0-\theta_E) = 0 \tag{11}$$

$$\frac{\sqrt{\mu/p}\left[-\cos L + \left(Q_2^2-Q_1^2\right)\cos L + 2Q_1Q_2\cos L - P_2 + 2P_1Q_1Q_2 + \left(Q_2^2-Q_1^2\right)P_2\right]}{1+Q_2^2+Q_1^2} + v_E \cos\theta_E + v_{\infty/E}\cos\gamma_0\cos(\beta_0-\theta_E) = 0$$

$$\frac{2\sqrt{\mu/p}[Q_2\cos L + Q_1 \sin L - P_2 + P_1Q_1 + Q_2P_2]}{1+Q_2^2+Q_1^2} - v_{\infty/E}\sin\gamma_0 = 0$$

Table 1 Partial list of predicted close approaches of comets and asteroids to within 8 lunar distances between 2001 and 2099

Object	Date	CA distance (lunar distance)
2340 Hathor	10/21/2086	2.22
2340 Hathor	10/21/2069	2.58
4660 Nereus	2/14/2060	3.12
4179 Toutatis	9/29/2004	4.06
4581 Asclepius	3/24/2051	4.76
4660 Nereus	2/4/2071	5.82
1991 OA	7/13/2070	5.82
1990 OS	11/16/2053	7.69
3200 Phaeton	12/14/2093	7.73
4179 Toutatis	11/5/2069	7.73

where all unsubscripted variables and elements refer to the orbit of the interceptor spacecraft, θ_E is the true longitude of the Earth, v_E is the circular velocity of the Earth, and all quantities are evaluated at $t = 0$.

The terminal constraint (10) yields the following three scalar equations:

$$r_A[\cos\theta_A\cos\Omega_A - \cos i_A\sin\Omega_A\sin\theta_A] - \frac{r\left[\cos L + \left(Q_2^2 - Q_1^2\right)\cos L + 2Q_1Q_2\sin L\right]}{1 + Q_2^2 + Q_1^2} = 0$$

$$r_A[\cos\theta_A\cos\Omega_A - \cos i_A\sin\Omega_A\sin\theta_A] - \frac{r\left[\sin L - \left(Q_2^2 - Q_1^2\right)\sin L + 2Q_1Q_2\cos L\right]}{1 + Q_2^2 + Q_1^2} = 0 \qquad (12)$$

$$r_A\sin i_A\sin\theta_A - \frac{2r[Q_2\sin L - Q_1\cos L]}{1 + Q_2^2 + Q_1^2} = 0$$

where all unsubscripted variables refer to the orbit of the interceptor spacecraft and all quantities are evaluated at t_{Final}.

Numerical Optimization

The problem is solved using the method of direct collocation with nonlinear programming.[8–10] In this solution method, the continuous problem is discretized by dividing the total time into segments whose boundaries are termed the system nodes. Each state is known only at discrete points: at the nodes and, depending on how the problem is formulated, at zero, one, or more points interior to a segment. Perhaps the best known collocation method is that of Hargraves and Paris,[8] employed in their trajectory optimization program OTIS. This version of the collocation method is both useful in itself and a good introduction to the process of discretizing a continuous problem and optimizing via nonlinear programming. We assume that the time history of the problem has been divided into N segments, each of width Δt_i. One such segment is shown in Fig. 1. We then assume that the state within a segment is approximated by a cubic polynomial (in time). The polynomial is uniquely determined by the endpoint information available: the parameter values of the states x_i and x_{i+1} and the system equation values $f_i(x_i, u_i, t_i)$ and $f_{i+1}(x_{i+1}, u_{i+1}, t_{i+1})$, where the various u are control variables, as shown in Fig. 1. It can be shown, using this cubic interpolant, that

$$x_C = -\tfrac{1}{2}(x_i + x_{i+1}) + (\Delta t_i/8)(f_i - f_{i+1}) \qquad (13)$$

is an approximate value for $x(t_C)$, where t_C is the center time $(t_{i+1} + t_i)/2$ and $\Delta t_i = t_{i+1} - t_i$. Similarly, it can be shown that the first time derivative of the cubic interpolant, evaluated at t_C, is

$$x'_C = -(3/2\Delta t_i)(x_i - x_{i+1}) - \tfrac{1}{4}(f_i + f_{i+1}) \qquad (14)$$

In the Hargraves and Paris method, x'_C is equated to the system equation evaluated at the center, i.e.,

$$x'_C = f_C(x_C, u_C, t_C) \qquad (15)$$

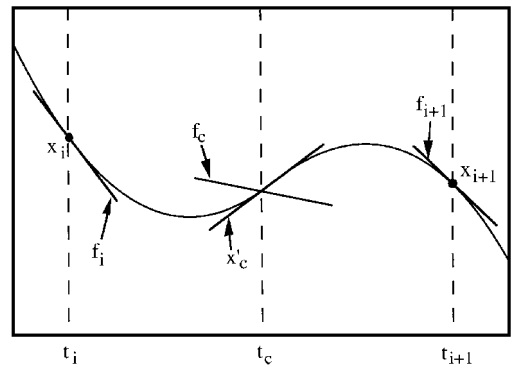

Fig. 1 Origin of the Hermite–Simpson constraint equations.

This is illustrated in Fig. 1; x'_C can be interpreted as the slope of the cubic at its center while the numerical value of f_C can also be interpreted as a slope. If Eq. (15) is satisfied, the two slopes will be the same, i.e., the cubic interpolant will satisfy the system differential equations at three points: the left and right nodes and the center.

Substituting Eq. (14) in Eq. (15) and isolating x_{i+1} yields

$$x_{i+1} = x_i + (\Delta t_i/6)[f_i + 4f_C + f_{i+1}] \qquad (16)$$

which is Simpson's quadrature rule, which must be satisfied for each of the n scalar state variables in the state vector x for each of the N segments into which the problem has been subdivided. The optimization problem has thus been converted into a nonlinear programming (NLP) problem; find the discrete states and controls $[x_1, u_1, x_2, u_2, \ldots, x_{N+1}, u_{N+1}]$ satisfying given initial and final state boundary conditions and $n \cdot N$ nonlinear constraint equations of form (16). Of course there may be upper and lower bounds on all of the state and control variables.

The preceding paragraphs describe just one elementary method for converting a continuous optimization problem into an NLP problem. There are many different ways of constructing the discretization, but all require some kind of implicit integration scheme, analogous to that of Eq. (16), i.e., some means of ensuring that successive values of the states closely approximate those that would result from a forward integration of the system equations for the given controls. Herman[11] and Herman and Conway[10,12] have shown how the implicit integration can be accomplished more accurately using constraints that are derived from integration rules of higher order than, and hence having smaller truncation error than, Simpson's rule. In this work, a fifth-degree Gauss–Lobatto integration rule,

$$\int_{t_i}^{t_{i+1}} f(t)\,\mathrm{d}t = \frac{\Delta t_i}{180}\left[9f(t_i) + 49f\left(t_C - \sqrt{\frac{3}{7}}\Delta t_i\right) + 64f(t_C) + 49f\left(t_C + \sqrt{\frac{3}{7}}\Delta t_i\right) + 9f(t_{i+1})\right] \qquad (17)$$

with an error function depending on $(\Delta t_i)^9$, as opposed to Simpson's rule, which has an error depending on $(\Delta t_i)^5$, is used implicitly. By analogy with the case for Simpson rule-derived constraints, the constaints that result from using (implicitly) the fifth-degree Gauss–Lobatto integration rule can be shown to be equivalent to approximating the state within the segment by a fifth-degree polynomial. Six quantities are needed to determine this polynomial; they are chosen to be x_i, f_i, x_c, f_c, x_{i+1}, f_{i+1} [where $x_i = x(t_i)$, $f_i = f(t_i)$, etc.], i.e., the values of the state and system equation at the left node, center, and right node of the ith segment, as illustrated in Fig. 2. Forcing the system differential equation to equal the slope of the polynomial at the two internal collocation points

$$x_1 = x\left[t_1 = t_c - \sqrt{\tfrac{3}{7}}(\Delta t_i/2)\right]$$
$$x_2 = x\left[t_2 = t_c + \sqrt{\tfrac{3}{7}}(\Delta t_i/2)\right] \qquad (18)$$

shown in Fig. 2 (rather than just the one, center point, in the method used by Hargraves and Paris), yields two system constraint equations per segment[10–12]:

$$C_{5,1}(x_{i+1}, x_C, x_{i+1}) = 0 = \tfrac{1}{360}\{(32\sqrt{21}+180)x_i - 64\sqrt{21}\,x_C + (32\sqrt{21}-180)x_{i+1} + \Delta t_i[(9+\sqrt{21})f_i + 98f_1 + 64f_C + (9-\sqrt{21})f_{i+1}]\}$$

$$C_{5,2}(x_{i+1}, x_C, x_{i+1}) = 0 = \tfrac{1}{360}\{(-32\sqrt{21}+180)x_i + 64\sqrt{21}\,x_C + (-32\sqrt{21}-180)x_{i+1} + \Delta t_i[(9-\sqrt{21})f_i + 98f_2 + 64f_C + (9+\sqrt{21})f_{i+1}]\} \quad (19)$$

Note that the sum of these two constraint equations recovers the original integration rule (17).

The optimizer is free to choose, for each segment, five control variables; u_i, u_1, u_c, u_2, u_{i+1}, i.e., the controls at the nodes and at the collocation points (including the center collocation point), as shown in Fig. 2. In this work the controls are free, i.e., there is no relationship specified between them as opposed to some collocation strategies in which the control time history can be represented by a polynomial or perhaps a linear function (in time). The discretized problem becomes a nonlinear programming problem, as described earlier for the case in which the implicit integration scheme is the simpler Hermite–Simpson rule. The parameters are thus the state variables (which are the six spacecraft orbit equinoctial variables + the thrust acceleration magnitude) at the nodes and center points of the segments and the control variables (the two thrust pointing angles) at the nodes, center point, and collocation points of each segment. There are three additional NLP variables: the final time t_f and the in-plane (β_0) and out-of-(ecliptic)-plane (γ_0) pointing angles that describe the direction of $\bar{v}_{\infty/E}$ following the impulsive Δv that allows the vehicle to escape from low-Earth orbit. The system nonlinear constraints are the defect equations (19), which enforce satisfaction of the differential equations, the initial condition constraints (11), and the conditions for interception (12).

The NLP problem is solved using the program NZSOL, an improved version of the program NPSOL.[13] For the two example trajectories determined in the next section, 20 segments were used to discretize the trajectory, yielding an NLP problem with 452 variables.

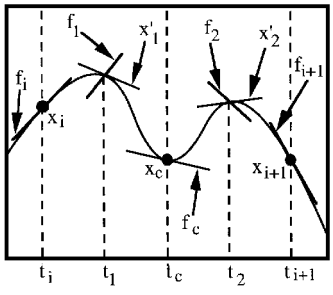

Fig. 2 Origin of the fifth-degree Gauss–Lobatto constraint equations.

More segments could be used, but the results for the state and control variable time histories, presented in the next section, show that all vary slowly and only over a small range, so that 20 segments capture quite well the system time history. This program requires an initial guess of the vector of parameters. The numerical optimization method used here has been quite robust when applied to a variety of orbit transfer problems.[9–12,14–16] The method was found to be less robust here than it has been for these other applications. However, it has been the experience of this researcher that once an initial guess that allows the optimizer to converge to an optimal trajectory has been determined, even one that has quite different initial and/or terminal conditions from the desired case, new optimal trajectories can be obtained using the converged solution as the new initial guess. Here the desired problem is solved by solving a succession of problems in which the orbit elements of the target asteroid of the existing solution are stepped toward those of the actual asteroid. As an example, for the first case described in the next section, the interception of 1862 Apollo, which has an inclination of 6.35 deg, the first converged solution was found for a fictitious target having zero inclination but an orbit of the same semimajor axis and eccentricity. This is a significantly easier problem to solve because two of the seven state variables, i.e., all of the various Q_1 and Q_2, are zero and can be set to zero in the optimizer. This solution was then used as an initial guess for a new problem with an inclination of 2 deg, which converged quickly, and the process continued until the desired problem was solved.

Examples

Several optimal trajectories have been found for the interception of actual Earth-crossing asteroids. The first asteroid considered, 1862 Apollo, is Earth crossing; i.e., it has a perihelion radius within 1 AU. Its orbit elements (on March 19, 1992) are $a = 1.47113$ AU, $e = 0.56015$, $i = 6.35488$ deg, $\Omega = 35.9564$ deg, $\omega = 285.6046$ deg, and $M = 156.7634$ deg (Ref. 5). Although Earth crossing, 1862 Apollo is not Earth approaching because, for the near future, the Earth is not near the ascending or descending node of the asteroid orbit when the asteroid is there. To create a test case with a target having at least the same orbit size, shape, and inclination of an Earth crosser, the longitudes of the ascending node and perihelion and the epoch mean anomaly were changed so that a near collision with the Earth would occur four months after the epoch time. Because dimensionless units are used in this analysis, i.e., $\mu = 1$ and the length unit is 1 AU, one time unit (TU) is equal to one year/2π so that four months = 2.101 TU.

An optimal trajectory has been found for the following initial conditions: $F_{\text{initial}} = 0.1$ AU/TU^2 $= 6.04 \cdot 10^{-5}$ g, $I_{sp} = 4000$ s, and $v_{\infty/E} = 0.0988$ AU/TU $= 2.942$ km/s. This initial thrust acceleration and specific impulse are representative of current electric propulsion technology. The hyperbolic excess velocity, provided by the chemical rocket motor at departure, is equal to what is required for a Hohmann transfer to Mars, so that it also is representative of current technology.

The optimal trajectory is shown in Fig. 3. Interception occurs at 1.634 TU (approximately 95 days) after launch. The optimizer

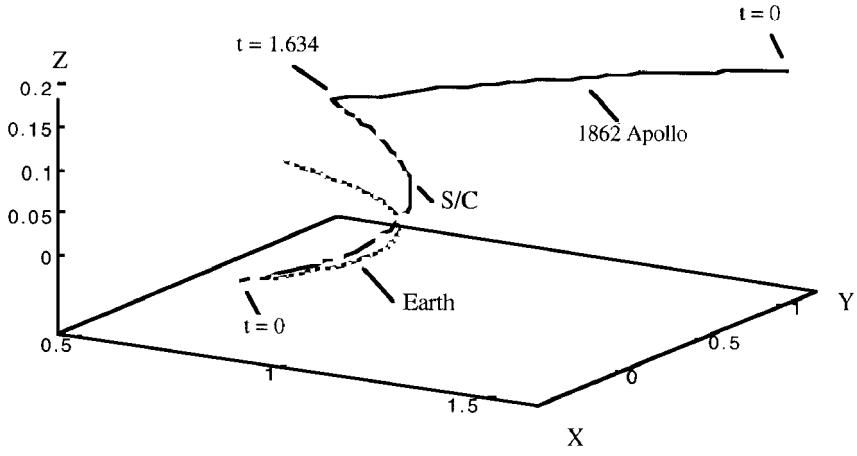

Fig. 3 Optimal trajectory for the interception of asteroid 1862 Apollo.

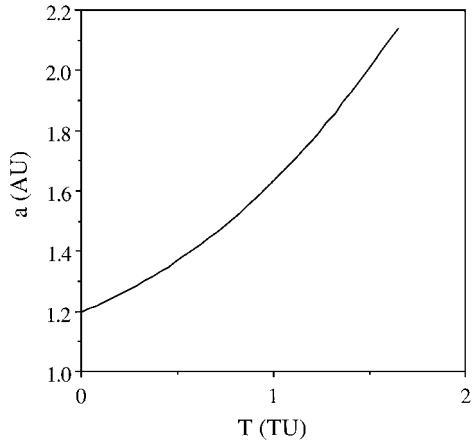

Fig. 4 History of the semimajor axis of the interceptor orbit shown in Fig. 2.

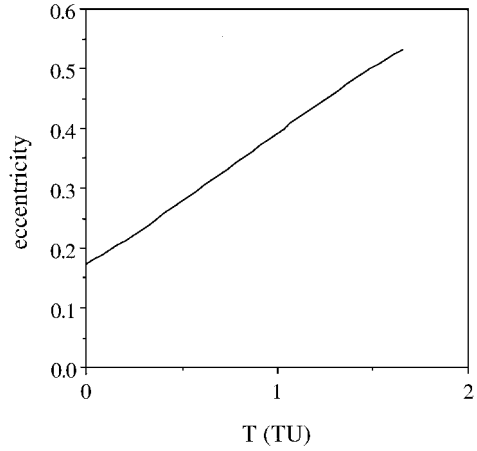

Fig. 5 History of the eccentricity of the interceptor orbit shown in Fig. 2.

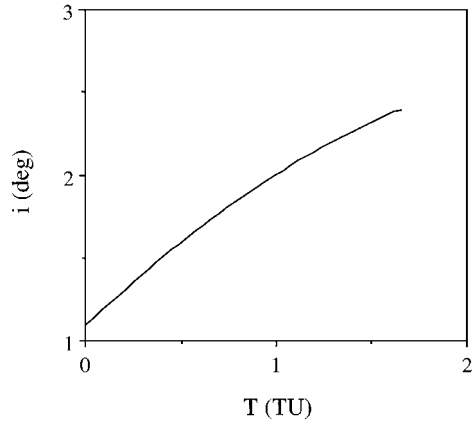

Fig. 6 History of the inclination of the interceptor orbit shown in Fig. 2.

chooses a direction for the $v_{\infty/E}$ vector through in-plane and out-of-(ecliptic)-plane pointing angles of -36.61 and $+11.80$ deg, respectively; i.e., the $v_{\infty/E}$ vector is chosen to point slightly above the ecliptic plane with a small radially inward component. The final thrust acceleration is 0.1989, almost twice the initial magnitude, indicating that almost half of the initial mass of the intercepting spacecraft must be propellant. The semimajor axis, eccentricity, and inclination of the interceptor orbit are shown in Figs. 4–6.

Optimal trajectories have also been found for the interception of Earth-approaching asteroid 1991RB. This asteroid has a much larger inclination than 1862 Apollo. As of Sept. 15, 1991, its orbit elements are $a = 1.4524$ AU, $e = 0.4846$, $i = 19.580$ deg, $\Omega = 359.599$ deg, $\omega = 68.708$ deg, and $M = 328.08$ deg (Ref. 5). This asteroid will approach the Earth to within 0.04 AU, or 15 lunar distances, on Sept. 19, 1998. It is assumed for the following example that launch from Earth takes place six months before the close approach, that is, on March 19, 1998. The true longitude of the Earth on that date is 177.21 deg. This is illustrated in Fig. 7. For this second example (referred to in Table 2 as case N), we assume that $F_{\text{initial}} = 0.14$ AU/TU$^2 = 8.46 \cdot 10^{-5}$ g, $I_{\text{sp}} = 4000$ s, and $v_{\infty/E} = 0.0333$ AU/TU $= 0.9807$ km/s. Note that the initial thrust acceleration has been increased by 40%, but the hyperbolic excess velocity decreased by 67% compared with the previous interception of 1862 Apollo.

The resulting optimal trajectory is shown in Fig. 8. The time of flight is 2.5096 TU = 145.9 days. The time histories of the interceptor orbit semimajor axis, eccentricity, and inclination are shown in Figs. 9–11. The in-(orbit)-plane and out-of-plane thrust pointing angles are shown in Figs. 12 and 13. The abscissa indicates node position, but this is linearly proportional to time, with the 80th node corresponding to the final time of 2.5096 TU.

Optimal trajectories for interception of 1991 RB have been determined for several different combinations of specific impulse, initial thrust acceleration, and hyperbolic excess velocity. The results are summarized in Table 2. The initial acceleration (in units of AU/TU^2) is the initial value of F, whose time variation is given by Eq. (8). The final acceleration provided in Table 2 allows the amount of propellant used on each trajectory to be calculated, as shown in the next section. The $v_{\infty/E}$ or hyperbolic excess velocity of escape is shown in each case, with 0.0988 AU/TU = 2.94 km/s, just what is required for a Hohmann transfer to Mars, as mentioned earlier. It results from an impulse applied in low Earth orbit, usually by the upper stage of the launch vehicle, and was chosen so that we may assume that the asteroid interceptor may be launched with an existing rocket. The

Table 2 Variation of flight time with initial thrust acceleration, specific impulse, and hyperbolic excess velocity (of Earth escape)

Case	Initial acceleration	I_{sp}, s	$v_{\infty/E}$, AU/TU	Flight time, days	Final acceleration
K	0.140	2000	0.0988	136.57	0.280
M	0.140	4000	0.0988	140.29	0.188
H	0.160	2000	0.0988	129.41	0.349
J	0.170	2000	0.0988	123.55	0.377
N	0.140	4000	0.0330	145.89	0.191
P	0.070	4000	0.0330	166.95	0.083

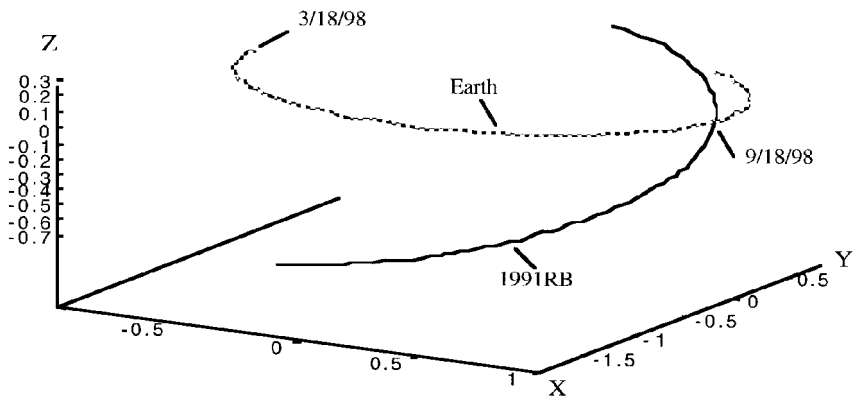

Fig. 7 Illustrating the close approach of asteroid 1991 RB on Sept. 18, 1998.

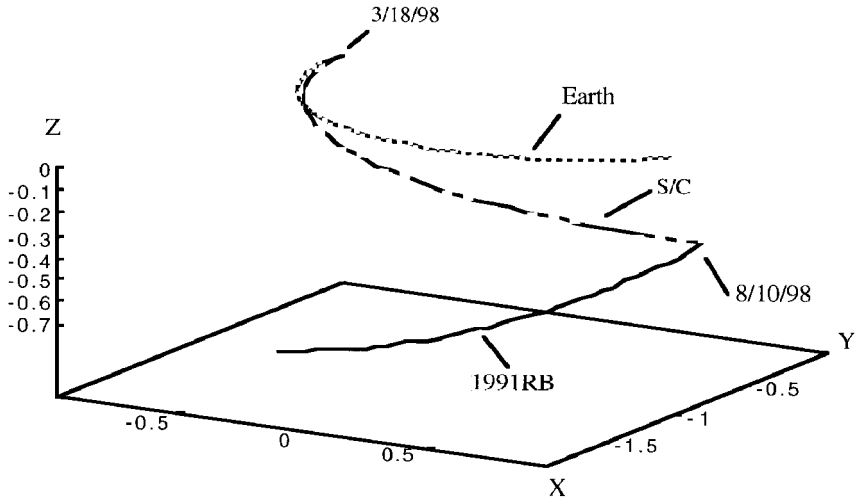

Fig. 8 Optimal trajectory for the interception of asteroid 1991 RB.

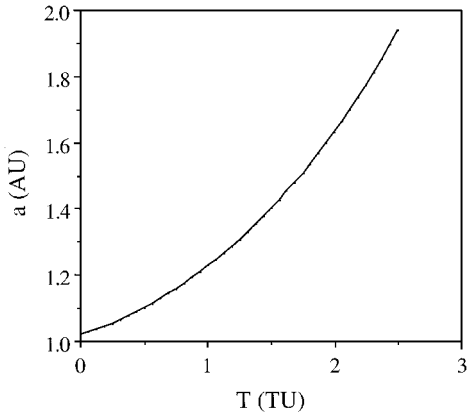

Fig. 9 History of the semimajor axis of the interceptor orbit shown in Fig. 7.

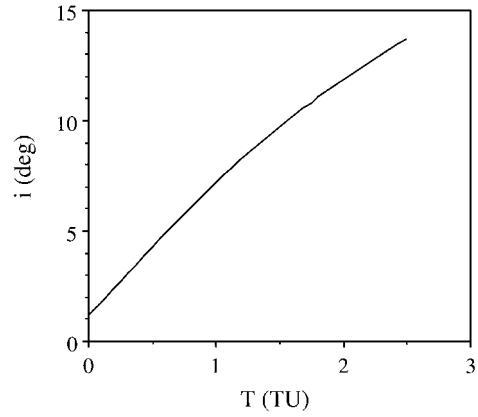

Fig. 11 History of the inclination of the interceptor orbit shown in Fig. 7.

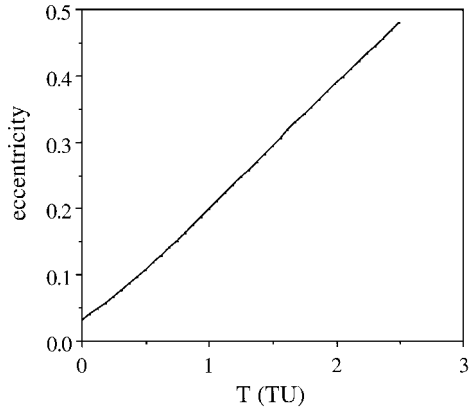

Fig. 10 History of the eccentricity of the interceptor orbit shown in Fig. 7.

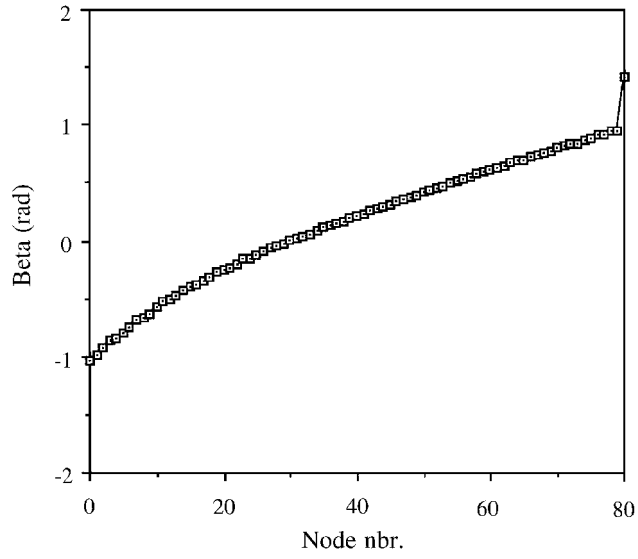

Fig. 12 History of the in-plane thrust pointing angle for the interceptor orbit shown in Fig. 7.

smaller $v_{\infty/E}$ assumed for cases N and P implies either launch with a smaller rocket or that the interceptor spacecraft is more massive than is assumed for the other cases.

Comparison with a One-Impulse Interception

The advantage of using continuous low-thrust propulsion is most apparent when the impulsive Δv required to duplicate the mission is determined. For the case described in the preceding paragraph (case N), the interception of 1991 RB, the time of flight, the date of departure (given in the preceding section), and the positions of departure and arrival are known. Determining the conic that connects these two points, in the same time of flight as for the low-thrust trajectory, but using impulsive velocity changes, is a Lambert problem. Solving Lambert's equation yields the semimajor axes of the elliptic sections connecting these two points in the given flight time.[17]

The trajectory with minimum required Δv has a semimajor axis $a = 1.3197$ AU. In terms of the Cartesian coordinate basis shown in Fig. 8 (in which the x–y plane is the ecliptic plane and the x axis points toward the first point in Aries), the heliocentric departure velocity vector required for a one-impulse interception is $\bar{v}_1 = [0.0931, -1.040, -0.3883]$. The velocity of the

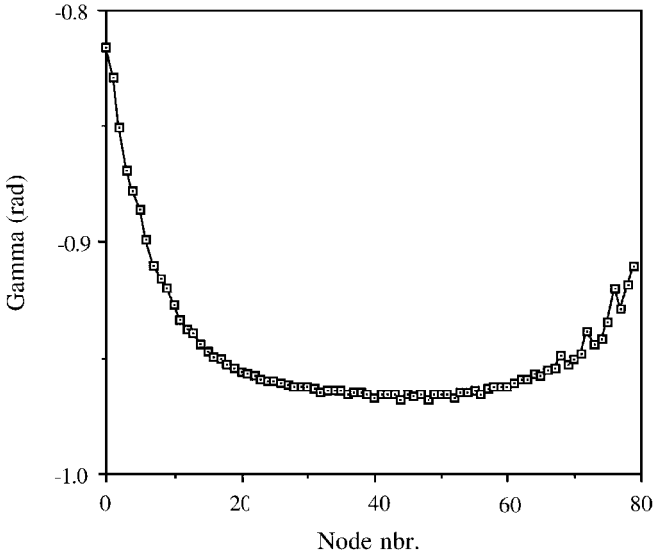

Fig. 13 History of the out-of-plane thrust pointing angle for the interceptor orbit shown in Fig. 7.

Earth on the date of departure is $\bar{v}_E = [-\sin\theta_E, \cos\theta_E, 0] = [-0.04857, -0.99882, 0]$. Case N assumes that the spacecraft is given an impulse in low Earth orbit that yields a $\bar{v}_{\infty/E}$ with magnitude 0.033 (=0.98 km/s) and that the direction of the v-infinity vector may be chosen by the optimizer, i.e., that the optimizer may choose the point over the Earth's surface that will be the perigee for the escape hyperbola. For an equitable comparison between the impulsive/low-thrust optimal trajectory and an all-impulsive trajectory, it must be assumed that the spacecraft using only impulsive thrust has the same v-infinity magnitude. Because the total velocity change required is in the direction of the vector $\bar{v}_1 - \bar{v}_E$, it is obviously optimal to have the small $\bar{v}_{\infty/E}$ in this direction. The single impulse that will place the spacecraft on the Lambert conic thus has magnitude $|\bar{v}_1 - \bar{v}_E| - |\bar{v}_{\infty/E}| = 0.382 = 11.37$ km/s.

This is a very substantial Δv, too large to be performed by a single-stage vehicle. As an example, if the impulse is provided by an optimal two-stage vehicle with engine specific impulses of 375 s and structural coefficient $\varepsilon = 0.12$ for each stage, the mass ratio at burnout of each stage becomes 4.689 and thus the first stage will have a mass of 79.59 times the payload mass and the second stage will have a mass of 8.43 times the payload mass.[17] The rocket mass is thus 88.03 times the payload mass. For an optimal two-stage vehicle consisting of a first stage having the characteristics of a Centaur RL 10A-4 ($\varepsilon = 0.116$ and $I_{sp} = 451$ s) and a second stage characteristic of a solid rocket motor ($\varepsilon = 0.10$ and $I_{sp} = 290$ s), the first stage will have a mass of 68.98 times the payload mass and the second stage 5.12 times the payload mass. The rocket mass is thus 74.10 times the payload mass. These two examples are intended to show only that a two-stage vehicle performing the same mission as the low-thrust spacecraft will be very massive, on the order of 75–90 times the mass of the payload.

In comparison, for the low-thrust trajectory of case N,

$$\frac{\text{final thrust acceleration}}{\text{initial thrust acceleration}} = \frac{m_0}{m_0 - m_{\text{FUEL}}} = \frac{0.191}{0.140}$$

so that the mass of the fuel used by the low-thrust motor is approximately 27% of the total initial mass of the vehicle. The current technology for electric propulsion is exemplified by the New Millenium DS-1 spacecraft, which produces 90 mN of thrust using 2.6 kW; it has a 71-kg power subsystem and 56 kg of ion propulsion hardware and structure, or approximately 1.4 kg of propulsion-related hardware per mN of thrust.[18] The initial thrust acceleration for case N of Table 2 is 0.14 in dimensionless units or 8.46×10^{-5} g or 0.83 mN/kg of initial mass. Thus with the technology used in the DS-1 spacecraft the asteroid interceptor would require $1.4(0.83) = 1.17$ kg of propulsion hardware plus 0.30 kg of fuel and tankage/kilogram of initial mass, i.e., the mission is infeasible.

A trajectory employing a smaller thrust, such as that of case P of Table 2, is feasible today; it would require only $1.4(0.415) = 0.58$ kg of propulsion hardware plus 0.17 kg of fuel and tankage per kilogram of initial mass, leaving approximately 25% of the initial mass for payload. Because the flight time for case P, which uses half of the intitial thrust acceleration of case N, is only 11% greater than that for case N, this is an attractive alternative. If we may assume that the technology will improve, reducing propulsion hardware to a mass fraction of perhaps 0.85 kg/mN from the 1.4 kg/mN needed for DS-1, a mission such as that of case N becomes just feasible and the case P mission payload fraction increases from 25 to 48%. Thus, albeit for a simplified analysis, the low-thrust asteroid interception vehicle payload should be a minimum of 25% of initial (postescape) mass with reasonable and even expected improvements in electric propulsion technology improving this to perhaps as much as 48%. The corresponding figure for chemical propulsion using a two-stage rocket is 1–2% with much less likelihood of significant improvement because the technology is mature.

Conclusions

The method of collocation with nonlinear programming has successfully solved the problem of finding minimum-time low-thrust trajectories for the interception of Earth-approaching asteroids. Continuous low-thrust propulsion provides a dramatic reduction in the amount of propellant required for the delivery of a given payload mass. The difference is so significant that, even if the low-thrust motor specific impulse is not as good as assumed, or the electric propulsion hardware more massive, or the chemical rocket performance and structural fraction better than assumed, this result will not change.

The combined impulsive/low-thrust trajectory used in this analysis, in which the impulse is used only for Earth departure to reduce the long flight time that would be required for a low-thrust escape from Earth orbit, appears to be very suitable for the cases used as examples here, in which launch takes place four to six months before the predicted close approach of the asteroid. If the danger of collision is known much earlier, a trajectory that uses only low-thrust propulsion may be feasible and would likely have additional advantages in total propellant required.

Future research might include the variation with distance from the sun of available power, and hence specific impulse for a solar-powered spacecraft, might require optimal rendezvous rather than interception, and, instead of minimizing flight time, might maximize the miss distance at Earth, which is the ultimate objective.

References

[1]Morrison, D., Chapman, C. R., and Slovia, P., "The Impact Hazard," *Hazards Due to Comets & Asteroids*, edited by T. Gehrels, Univ. of Arizona Press, Tucson, AZ, 1994, pp. 59–91.

[2]Adushkin, V. V., and Nemchinov, I. V., "Consequences of Impacts of Cosmic Bodies on the Surface of the Earth," *Hazards Due to Comets & Asteroids*, edited by T. Gehrels, Univ. of Arizona Press, Tucson, AZ, 1994, pp. 721–778.

[3]Yau, K., "Meteorite Falls in China and Some Related Human Casualty Events," *Meteoritics*, Vol. 29, No. 6, 1994, pp. 864–871.

[4]Hills, J. G., Nemchinov, I. V., Popov, S. P., and Taterev, A. V., "Tsunami Generated by Small Asteroid Impacts," *Hazards Due to Comets & Asteroids*, edited by T. Gehrels, Univ. of Arizona Press, Tucson, AZ, 1994, pp. 779–790.

[5]Rabinowitz, D. L., et al., "The Population of Earth-Crossing Asteroids," *Hazards Due to Comets & Asteroids*, edited by T. Gehrels, Univ. of Arizona Press, Tucson, AZ, 1994, pp. 285–312.

[6]*MICA, An Interactive Astronomical Almanac*, U.S. Naval Observatory, Washington, DC, 1989.

[7]Battin, R. H., *An Introduction to the Mathematics and Methods of Astrodynamics*, AIAA Education Series, AIAA, New York, 1987, pp. 490–494.

[8]Hargraves, C. R., and Paris, S. W., "Direct Trajectory Optimization Using Nonlinear Programming and Collocation," *Journal of Guidance, Control, and Dynamics*, Vol. 10, No. 4, 1987, pp. 338–342.

[9]Enright, P. J., and Conway, B. A., "Discrete Approximations to Optimal Trajectories Using Direct Transcription and Nonlinear Programming," *Journal of Guidance, Control, and Dynamics*, Vol. 15, No. 4, 1992, pp. 994–1002.

[10]Herman, A. L., and Conway, B. A., "Direct Optimization Using Collocation Based on High-Order Gauss-Lobatto Quadrature Rules," *Journal of Guidance, Control, and Dynamics*, Vol. 19, No. 3, 1996, pp. 592–599.

[11]Herman, A. L., "Improved Collocation Methods Used for Direct Trajectory Optimization," Ph.D. Thesis, Dept. of Aeronautical and Astronautical Engineering, Univ. of Illinois, Urbana, IL, Sept. 1995.

[12]Herman, A. L., and Conway, B. A., "Direct Solutions of Optimal Orbit Transfers Using Collocation Based on Jacobi Polynomials," AAS/AIAA Space Flight Mechanics Meeting, AAS Paper 94-126, Cocoa Beach, FL, Feb. 1994.

[13]Gill, P. E., "User's Guide for NZOPT 1.0: A Fortran Package for Nonlinear Programming," McDonnell Douglas Aerospace, Huntington Beach, CA, April 1993.

[14]Enright, P. J., "Optimal Finite-Thrust Spacecraft Trajectories Using Direct Transcription and Nonlinear Programming," Ph.D. Thesis, Univ. of Illinois, Urbana, IL, 1991.

[15]Scheel, W. A., and Conway, B. A., "Optimization of Very-Low-Thrust, Many Revolution Spacecraft Trajectories," *Journal of Guidance, Control, and Dynamics*, Vol. 17, No. 6, 1994, pp. 1185–1192.

[16]Tang, S., and Conway, B. A., "Optimization of Low-Thrust Interplanetary Trajectories Using Collocation and Nonlinear Programming," *Journal of Guidance, Control, and Dynamics*, Vol. 18, No. 3, 1995, pp. 599–604.

[17]Prussing, J. E., and Conway, B. A., *Orbital Mechanics*, Oxford Univ. Press, New York, 1993.

[18]"Deep Space 1 Spacecraft Specifications," Spectrum Astro Corp., Gilbert, AZ, 1997.